Journal of Biomedical Optics

BiomedicalOptics.SPIEDigitalLibrary.org

Optical properties of rabbit brain in the red and near-infrared: changes observed under *in vivo*, postmortem, frozen, and formalin-fixated conditions

Andreas Pitzschke
Blaise Lovisa
Olivier Seydoux
Matthias Haenggi
Markus F. Oertel
Matthieu Zellweger
Yanik Tardy
Georges Wagnières

SPIE.

Optical properties of rabbit brain in the red and near-infrared: changes observed under *in vivo*, postmortem, frozen, and formalin-fixated conditions

Andreas Pitzschke,[a] Blaise Lovisa,[a,b] Olivier Seydoux,[a] Matthias Haenggi,[c] Markus F. Oertel,[d] Matthieu Zellweger,[a] Yanik Tardy,[b] and Georges Wagnières[a,*]
[a]Swiss Federal Institute of Technology, Institute of Chemical Sciences and Engineering, Station 6, Lausanne CH-1015, Switzerland
[b]Medos International Sàrl, a J&J Company, Chemin Blanc 38, Le Locle CH-2400, Switzerland
[c]University of Bern, Department of Neurosurgery, Bern University Hospital, Inselspital, Bern CH-3010, Switzerland
[d]University of Bern, Department of Intensive Care Medicine, Bern University Hospital, Inselspital, Bern CH-3010, Switzerland

Abstract. The outcome of light-based therapeutic approaches depends on light propagation in biological tissues, which is governed by their optical properties. The objective of this study was to quantify optical properties of brain tissue *in vivo* and postmortem and assess changes due to tissue handling postmortem. The study was carried out on eight female New Zealand white rabbits. The local fluence rate was measured in the VIS/NIR range in the brain *in vivo*, just postmortem, and after six weeks' storage of the head at −20°C or in 10% formaldehyde solution. Only minimal changes in the effective attenuation coefficient μ_{eff} were observed for two methods of sacrifice, exsanguination or injection of KCl. Under all tissue conditions, μ_{eff} decreased with increasing wavelengths. After long-term storage for six weeks at −20°C, μ_{eff} decreased, on average, by 15 to 25% at all wavelengths, while it increased by 5 to 15% at all wavelengths after storage in formaldehyde. We demonstrated that μ_{eff} was not very sensitive to the method of animal sacrifice, that tissue freezing significantly altered tissue optical properties, and that formalin fixation might affect the tissue's optical properties. [DOI: 10.1117/1.JBO.20.2.025006]

Keywords: light dosimetry; tissue optics; optical coefficients; VIS/NIR; rabbit brain; formalin; photobiomodulation.

Paper 140700R received Oct. 24, 2014; accepted for publication Jan. 29, 2015; published online Feb. 23, 2015.

1 Introduction

Numerous models exist to predict the photon transport in biological tissues, yet their accuracy ultimately depends on how well the optical properties of the tissues are known.[1] Since their determination *in vivo* is complicated, they are often determined postmortem and *ex vivo* and then applied for *in vivo* applications accordingly. Nevertheless, tissue preparation and storing techniques may frequently alter these properties, e.g., after dissection when tissue is processed and prepared for measurement by soaking in saline solution leading to partial removal of hemoglobin.[2,3] Other alterations may result from tissue drying,[4] e.g., during lengthy preparation or measurement procedures. Furthermore, tissue heating, e.g., for easier removal of the epidermis, is known to affect the optical properties.[5–7] Histological processing, such as freezing[3,8] and fixation,[9,10] for sample preparation or cutting and storing could also alter optical properties. When using nonhuman tissue for comparative studies, the method of animal sacrifice may also have an impact on the optical properties, e.g., by removal of hemoglobin when exsanguinating the animal.

The objective of the present study was to quantify for the first time how the effective light attenuation in brain tissue changes between the *in vivo* and postmortem status, and how it could be affected by histological tissue processing and the animal sacrifice itself. These results shall give considerable insight on how postmortem optical coefficients found in literature and measured on tissue, obtained after fixation or even from the abattoir, can be properly interpreted and used for *in vivo* situations. Unfortunately, very little is known about the changes in the optical coefficients of postmortem tissue. In previous studies, storage effects were investigated on tissue derived from liver,[3,11] jejunum,[8] myocardium,[9] dermis,[12,13] and aorta.[4,8] To our knowledge, there are hitherto no comparable studies on brain tissue.

In this study, a rabbit model was chosen. The rabbit brain is sufficiently large for this kind of measurement and it can be easily accessed with the measurement probes. We assumed that changes in the optical properties due to the above-mentioned tissue treatment should be representative of human brain tissue, since tissue optical properties of rodent brain are comparable to those of human encephalon.[14–16] The light distribution was measured at three different wavelengths in the VIS/NIR spectrum by the use of optical fiber based light diffusers and isotropic probes. Measurements were performed *in vivo*, postmortem after animal sacrifice by exsanguination or KCl injection, and after long-term tissue storage for six weeks in either formalin or frozen at −20°C. The optical coefficients, effective attenuation, absorption and reduced scattering were derived by fitting the experimental data. Finally, the influence of the experimental constraints on the measured data was interpreted by Monte Carlo simulations.[17–19]

*Address all correspondence to: Georges Wagnières, E-mail: georges.wagnieres@epfl.ch

1083-3668/2015/$25.00

2 Materials and Methods

2.1 *Animal and Tissue Handling*

All animal studies were approved by the Animal Care and Experimentation Committee of the Canton of Bern, Switzerland, and followed the Swiss national guidelines for the performance of animal experiments. We examined eight female New Zealand white rabbits at least 15 weeks old and weighing 3.5 to 4 kg (Charles River Laboratories GmbH, Sulzfeld, Germany). They were housed in the core animal facilities of the University of Bern with a 12/12 h light/dark cycle at 22°C and with food and water *ad libitum*.

For anesthesia, animals received a premedication of 35 mg/kg ketamine and 10 mg/kg xylazine, followed by isoflurane 2 to 5% and fentanyl 50 μg/kg/h during the whole course of the measurements. Euthanasia was carried out for four animals by bleeding from the femoral artery followed by injection of concentrated 2 mmol/ml KCl solution to stop the heart from beating, and for the remaining four animals by direct injection of KCl. After the *in vivo* and postmortem measurements, the rabbit heads were sawed off and kept either frozen at -20°C or in neutral-buffered 10% formaldehyde solution (Hospital Pharmacy, Inselspital, Bern, Switzerland).

X-ray images of the catheter locations in the skull were documented with a portable x-ray system (Philips, BV Pulsera R1.2, Eindhoven, The Netherlands).

2.2 *Experimental Setup for Light Delivery and In Situ Measurements of the Fluence Rate*

Light was delivered through a dedicated cylindrical diffuser of 20 mm length and 1 mm diameter (RD20, Medlight SA, Ecublens, Switzerland), whose power output was calibrated with an integrating sphere (LMS-200, 20 in. diameter, Labsphere Inc., New Hampshire) before and after experiments. The diffuser was connected to laser diodes emitting at 635 nm (Ceralas PDT, 635/4W/400 μm, CeramOptec GmbH, Bonn, Germany), 671 nm (RLTMRL-671-1W), or 808 nm (RLTMDL-808-5W, Roithner Lasertechnik GmbH, Vienna, Austria). The power output of each laser was calibrated with a frontal light diffuser (FD1, Medlight SA) and powermeter (detector 818P-010-12, driver 1918-R, SpectraPhysics Newport, California) prior to measurements.

Four catheters (iCAT-2.0-200, OD 2.0 mm, Medlight SA) per animal were placed transcranially and fluoroscopically via burr-holes into defined locations in the brain [see Fig. 1(b)]. They were left in place during and after euthanasia to avoid changes in catheter positions. Catheter locations were defined by a solid guiding plate with a 3×3 cm^2 matrix of evenly spaced holes (6 mm hole–hole distance). Catheter positions were chosen to fit to the shape of the rabbit brain ensuring different catheter-to-catheter distances (four to five different distances in the range of ~6 to 15 mm). The same burr-holes and matrix positions were used for the measurements after long-term storage of

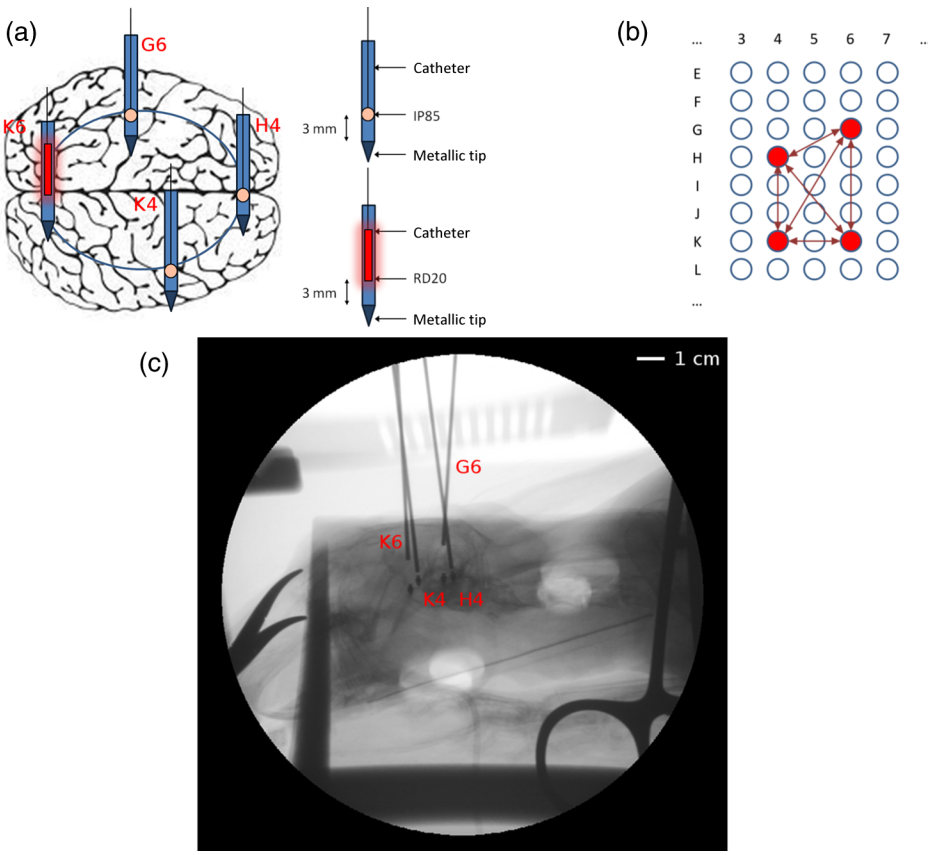

Fig. 1 Experimental setup. (a) and (b) schematic showing the arrangement of catheters inserted in the brain containing either light diffuser or isotropic probes. (c) presents an x-ray image taken from the sagittal plane of the rabbit brain. Catheters labeled in red containing either light diffuser or isotropic probe were inserted in the brain such that maximal six relative distances were covered.

the skulls. The guiding plate was fixed to the operation table above the head of the rabbit such that catheter alignment was ensured by two points, the burr-holes in the skull and the holes in the plate. Isotropic probes with a diameter of 0.85 mm (IP85, Medlight SA) were used for the measurement of the local fluence rate. Their response was measured with a calibrated FD1 at all wavelengths before and after the experiment.

A light diffuser or isotropic probe was inserted in the catheter's lumen to assess the light transmission between the different catheter locations. The light diffuser spanned the full transverse axis of the rabbit brain, leading to symmetric irradiation of the surrounding tissue in the transverse plane. The fluence rate was measured simultaneously at each probe location with a calibrated multichannel photometer (OP710-IN, Opto-Test Corporation, Camarillo, California). Measurements were carried out for a minimum of five different positions in the catheters, i.e., in the transverse plane of the brain, typically spaced at intervals of 3 mm, to avoid biased signals due to local inhomogeneities in the tissue, such as blood vessels. During this measurement, the light diffuser remained in place. The influence of the catheter on the fluence rate measurement, i.e., light attenuation and wave guide effects, was determined by illuminating the isotropic probes with and without the catheter in the integrating sphere or directly by a frontal light diffuser. The changes in the measured fluence rate due to the presence of a catheter were <5% and, therefore, negligible.

Measurements were repeated by rotating light diffuser and isotropic probes through all different catheters [Figs. 1(a) and 1(b)] in order to improve statistics, minimize effects of local tissue inhomogeneities, and reduce the influence of boundary effects due to the finite brain size on the measured data. During reallocation of diffuser and probes, the laser was switched off to prevent unnecessary heating of the brain tissue around the light diffuser. In only one single case an accelerated heartbeat of the animal was noticed during measurements at 635 nm. It is not clear whether this effect was stimulated by the light itself, by heat from the absorbed light, or a combination of both mechanisms.

The fluence rate was measured in the living animal, after euthanasia, and six weeks after long-term storing of the animal's head fixed by either formaldehyde or freezing. Thawing of the frozen tissue samples was assured by placing them into a fridge at 4°C ~12 h prior to measurements. The measurements were carried out in all rabbits at 635, 671, and 808 nm for all tissue conditions, except for one rabbit where there was no measurement at 671 nm for the *in vivo* and postmortem conditions. A second animal died before *in vivo* measurements could be performed.

The influence of blood on the postmortem light propagation was assessed by comparing results from a control population of four rabbits euthanized with an injection of KCl and a study population of four rabbits where the blood was drained out during euthanasia. It is noteworthy that only 40 to 50% of the total amount of blood could be exsanguinated. For estimating storage effects on the tissue optical properties, two rabbit heads of each group, i.e., euthanized by KCl or exsanguination, were slowly frozen to −20°C. The remaining two rabbit heads of each group were fixed in formalin. In order to assure optimal comparability of experimental results with the data reported in the literature, both long-term storage techniques were chosen to be as similar as possible to the methods applied previously to human tissues and cadavers.

2.3 *Data Processing*

2.3.1 *Diffusion model for a cylindrical diffuser*

An analytical model based on the diffusion approximation was used to describe the propagation of light in the rabbit brain. The steady-state expression for photon diffusion in a tissue is given by[20]

$$(\Delta - \mu_{\text{eff}}^2)\phi(r) = -q(r)/D, \tag{1}$$

with $\phi(r)$ being the fluence rate (mW/cm^2), $\mu_{\text{eff}} = \{3\mu_a[\mu_a + \mu_s(1-g)]\}^{1/2}$ the effective attenuation coefficient (cm^{-1}), $D = \mu_a/\mu_{\text{eff}}^2$ the optical diffusivity (cm), and q the diffusive photon density (mW/cm^3). The absorption and scattering coefficients, μ_a (cm^{-1}) and μ_s (cm^{-1}), express the probability for a photon to be absorbed or scattered on a given path length. In the diffusion regime, the anisotropic scattering is usually simplified to the isotropic case by defining the reduced scattering coefficient $\mu_s' = \mu_s(1-g)$ (cm^{-1}), where g is the scattering anisotropy described by the Henyey-Greenstein phase function.[21] The solution of Eq. (1) for the fluence rate of an infinitely long cylindrical light diffuser in the cylindrically symmetric case[22] is given by

$$\phi(r) = \frac{P/2\pi a}{D\mu_{\text{eff}} K_1(\mu_{\text{eff}}\, a)} K_0(\mu_{\text{eff}}\, r), \tag{2}$$

where P is the optical power per unit length (mW/cm) of the light diffuser with radius a (cm). K_0 and K_1 are the modified Bessel K functions of the zero and first order, respectively. The distance from the diffuser axis is expressed as r (cm).

The relative distances of the isotropic probe positions with respect to the diffuser axis, r, were determined from x-ray images taken after catheter insertion into the brain and prior to the measurements. After the long-term storage of the rabbit head, a second set of x-ray images was taken after reinsertion of the catheters. The metallic catheter tips and stylets were used to identify the catheter positions on the images from the sagittal and axial planes. Stylet diameter, catheter tips, and the hole distances in the matrix holding the catheters were measured on the x-ray images and an average value was used to determine the transformation from image pixels to real space. The average resolution of the images was 0.2 to 0.25 mm/pixel, which yields an uncertainty in absolute positions of ~1 mm when taking a usual value of 3 to 4 pixels as the uncertainty of the manual readout. The two three-dimensional geometries of the catheter positions, i.e., during the measurements *in vivo* / postmortem and after long-time storage, were reconstructed for each animal.

The experimental data were fitted by Eq. (2) using MATLAB®'s least-square Levenberg-Marquardt algorithm *lsqnonlin* (R2013a, The MathWorks, Inc., Natick, Massachusetts). By using the absolute calibration of the light source, the fluence rate at the light diffuser surface was calculated from Eq. (2) and imposed to the fit as a boundary condition. This constraint was updated during each iteration by recomputing its value based on the new set of fitted optical properties. This procedure was validated by fitting sets of artificial data with predefined μ_a and μ_s' simulating the experimental conditions, i.e., typical distances to the source and data scattering (Gaussian distribution of noise). The accuracy in μ_{eff} obtained by the fit was found to be within ±10%. For sets of μ_a and μ_s' yielding $\mu_{\text{eff}} < 0.2$ mm^{-1}, errors in the fitted μ_{eff} increased, consequently, up to 15%. In general, μ_a was underestimated and μ_s' overestimated, and the

combination of small μ_a (~0.01 mm^{-1}) and large μ_s' (~5 mm^{-1}) leads to the largest uncertainties. Typical fit values of the optical coefficients for rabbit brain were found to be $\mu_a \sim 0.03$ to 0.13 mm^{-1} and $\mu_s' \sim 0.5$ to 1.4 mm^{-1} at various wavelengths, hence in the range of highest fitting accuracy. The correlation between the two fitting parameters ranged from 0.3 to 0.6 and usually decreased with increasing wavelength; therefore, absolute values of absorption and reduced scattering coefficients need to be considered with caution.

The diffusion model is valid if (1) the medium is very diffusing, i.e., $\mu_a \ll \mu_s'$, the light distribution is studied (2) far enough from the light distributor, typically at a distance longer than the effective mean free path defined as $(\mu_s + \mu_a)^{-1}$, and (3) in a semi-infinite media. Despite the high correlation between absorption and reduced scattering coefficient, the fitting results indicated $\mu_s'/\mu_a \sim 10$ satisfying the first condition. The second condition was also valid, since measurements were carried out at distances $r > 5$ mm, whereas $(\mu_s' + \mu_a)^{-1} \sim 1/\mu_s' \sim 0.1$ mm. On the contrary, measurements at distances $r \geq 15$ mm came close to the skull violating the third condition, so that Monte Carlo simulations became necessary to investigate possible boundary effects.

2.3.2 *Determination of the validity domain of the analytical model by Monte Carlo simulations*

In some cases, fluence rate measurements showed deviations from the common behavior of exponential decline (data not shown here). These deviations were significantly higher values of fluence rate at distances of $r \geq 15$ mm as expected, especially at smaller wavelengths. Monte Carlo simulations were carried out to compute the fluence rate at the brain/skull/air boundary to explain this phenomena. The code mesh-based Monte Carlo (MMC) (Ref. 23) was used to simulate the photon propagation through a tetrahedral mesh generated by the *iso2mesh*-toolbox.[24]

A generic brain model was built out of ellipsoids representing the brain, cerebro-spinal fluid (CSF), and skull. Dimensions of the rabbit brain were taken from the literature[25] (semi-principal axis was equal to $18.5 \times 11 \times 8$ mm^3). The thickness of the CSF and skull layer enveloping the brain were approximated from the x-ray images and set to 1 mm. Only the catheter containing the light diffuser was modeled as an air-filled cavity with a Lambertian emission profile (10^8 photons). Several simulations were carried out for different light source positions simulating the conditions of the experiments. During the simulations, the cylindrical light diffuser was aligned parallel to the smallest semiprincipal axis and (1) central in the ellipsoid, (2) lateral from the ellipsoid center, i.e., left or right side of the skull, and (3) posterior of the ellipsoid center, i.e., toward the jaw or neck. Since, to our knowledge, no optical tissue parameters are available for rabbit brain and skull, they were taken for human tissue instead (see Table 1). The same coefficients were used to cross-verify the analytical solution, Eq. (2), with the results from Monte Carlo simulations.

Table 1 Optical properties used for simulating the boundary effects via the Monte Carlo model. The properties for scalp/skull and cerebrospinal fluid (CSF) were taken from a reference for human tissue in the near-infrared.[26] Those for the brain were based on human pons[7] at 808 nm reproducing best the measured μ_{eff}.

Tissue type	μ_a (cm^{-1})	μ_s' (cm^{-1})	μ_s (cm^{-1})	g	n
Scalp and skull	0.19	8.58	78	0.89	1.37
CSF	0.04	2.97	27	0.89	1.37
Brain	0.60	6.40	80	0.92	1.37

3 Results

3.1 *Fluence Rate Measurements and Interpretation by Monte Carlo Simulations*

The exponential decay of the fluence rate as a function of the distance between the source and detector, as described by Eq. (2), was reflected in the experimental data at all wavelengths. Furthermore, the light attenuation, and consequently the effective attenuation coefficient, was highest at 635 nm and became smaller at increasing wavelengths. These observations are represented in Fig. 2(a) by typical profiles of the measured fluence rate and their fit yielding μ_{eff}. However, at large distances r between light source and detector, i.e., $r > 10$ mm, measurements revealed a two to five times higher value for the fluence rate than expected from theory. The effect was most prominent at 635 nm and became less distinguishable at longer wavelengths, which may result from a higher μ_s' at shorter wavelengths.

This behavior was quantified by simulating the fluence rate at the boundary of the rabbit brain by the Monte Carlo method. The simulated fluence rate at the midplane of the ellipsoid representing the rabbit brain is shown in Fig. 2(b) together with the fluence rate obtained from the analytical expression. There was a good agreement between results from the Monte Carlo simulation for a semi-infinite cylinder and the analytical solution from diffusion approximation. Results for the generic rabbit brain, where the light diffuser was positioned either centered, lateral, or posterior, were in agreement with the analytical solution for $1 \leq r \leq 10$ mm. On the contrary, at $r > 10$ mm, local deviations of the fluence rate from the analytical expression became prominent. These were also noticeable in the experimental data: they are a consequence of the brain boundaries imposed by the semiprincipal axis of the ellipsoid. The usually larger fluence rate at the brain boundary originates from backscattering of photons. First, the CSF with its small μ_{eff} is acting as a light cavity leading to a higher photon flux at the brain/CSF transition. Second, the refractive-index mismatch at the skull/air transition is partially backscattering the photons. The fluence rate beyond the skull/air transition drops quickly as there are no photon scattering or absorption events.

Furthermore, we noted that the analytical expression overestimated the fluence rate at the diffuser surface by up to 15% compared to the simulations. However, this effect was negligible considering the large scatter in the experimental data and the fact that the fluence rate at the diffuser surface, given as boundary condition to the fitting procedure, was recomputed during each iteration.

The boundary effects raised the necessity to filter the experimental data for artifacts at large distances, $r > 10$ cm, prior to fitting. A general trend was that these effects became more prominent at smaller wavelengths, i.e., 635 and 671 nm. This is due to the increased scattering at smaller wavelengths, since $\mu_s' \propto \lambda^{-\alpha}$ with $\alpha > 0$ as described by the Mie theory of scattering.[27] Despite the boundary effects, the good agreement between the analytical approach and simulation, however,

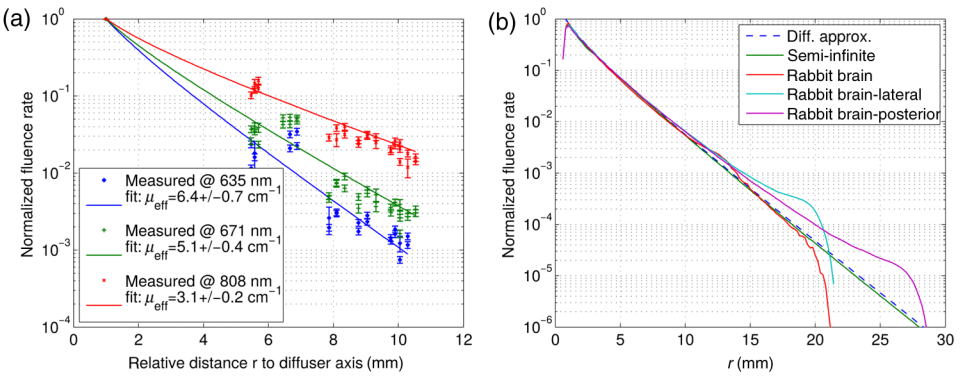

Fig. 2 Measured and simulated fluence rate normalized to the fluence rate at the diffuser surface. (a) shows the *in vivo* normalized measured data fitted by the analytical expression. The fit was constrained by setting the fluence rate at the diffuser surface to the value computed by Eq. (2) for injected laser light power measured prior to the experiment. (b) shows the normalized fluence rate simulated by MMC. The dashed blue line is the fluence rate obtained from Eq. (2) whereas the solid colored lines are the fluence rates in different geometries: a semi-infinite cylinder with the finite light diffuser along the cylinder axis or the generic brain with the light diffuser in one of the semiprincipal axis, lateral or posterior to it.

suggested Eq. (2) to be an appropriate choice for modeling the data obtained in our experimental conditions.

3.2 *Influence of Tissue Storing on the Optical Coefficients*

The measured effective light attenuation coefficient μ_{eff} for rabbit brain is presented in Fig. 3(a) for all experimental conditions and in Fig. 3(b) for all tissue conditions, i.e., *in vivo*, postmortem, and after long-term storage at −20°C or formalin-fixated. We compared the median of μ_{eff}, and not the mean, because it is less sensitive to skewed distributions of the attenuation values. Standard deviations were computed from the median absolute deviation. The effective light attenuation coefficients for all tissue conditions together with its uncertainties are listed in Table 2.

The groups postmortem, frozen, and formalin-fixated, shown in Fig. 3(b), contain data from animals euthanized in both ways, i.e., either by exsanguination or injection of KCl, since little changes in μ_{eff} were observed as function of the sacrifice method. The data suggest that the effect of bleeding on μ_{eff} was negligible in our series. Cerebral blood circulation may have been sufficiently sustained prior to euthanasia, since 50 to 60% of the total blood volume remained in the animal during the bleeding procedure. Furthermore, light absorption by oxy- or deoxyhemoglobin was much larger at wavelengths <600 nm, such that a lower blood volume than normal may influence only little μ_{eff} at wavelengths >600 nm.

Under all predetermined tissue conditions applied, μ_{eff} decreased as a function of the wavelength. This wavelength dependency was attributed to a decreasing value of μ_s' at increasing wavelengths according to the Mie scattering theory as well as to a decrease of μ_a, especially in deoxyhemoglobin. These findings are in agreement with results reported for human brain tissue.[7]

The relative changes in the effective attenuation coefficient, $\delta\mu_{\text{eff}} = (\mu_{\text{eff}} - \mu_{\text{eff}}^*)/\mu_{\text{eff}}^*$, where μ_{eff}^* stands for the *in vivo* condition, are shown in Fig. 3(c). We observed that the decrease in μ_{eff} between *in vivo* and postmortem conditions was largest at 635 nm, which was up to 10%, whereas at higher wavelengths, it was only 5%.

After storage of the rabbit heads at −20°C for six weeks, μ_{eff} decreased, on average, by 15 to 25% at all wavelengths [Fig. 3(c)]. Which coefficient was the crucial factor, however, remained controversial. Although the absolute values of fitted absorption and reduced scattering coefficient partly had a high cross-correlation and, thus, did not represent a unique solution of Eq. (2) to the experimental data, relative changes in these parameters between different tissue conditions may indicate which coefficient is most affected. These changes, when passing from postmortem to frozen conditions, yield a decrease in μ_a by ∼30% at all wavelengths and a decrease of μ_s' by ∼10% with the smallest effect at 808 nm (see also Table 2).

The effective attenuation coefficient after formalin fixation is shown in Fig. 3(b) and its relative changes in Fig. 3(c). Our measurements showed an increase in μ_{eff} by 5 to 15% after having stored the rabbit heads in formaldehyde for six weeks. The relative changes in the optical coefficients indicate that μ_a increased by ∼15% and μ_s' by ∼5% at all wavelengths.

4 Discussion

4.1 *Tissue Freezing*

Tissue freezing is an elegant method to store and transport tissue samples, but was shown to significantly alter tissue optical properties.[3,8,13] So far, there are only a few studies investigating these effects, and a summary of their results together with ours can be found in Table 3. In general, it is reported that tissue freezing, either at −20°C or 77 K, reduces the effective attenuation coefficient. However, it remains unclear from these results which coefficient, absorption or reduced scattering, is more affected by the freezing procedure.

On a microscopic level, we expected freezing to cause changes in the tissue structure. Depending on the freezing and thawing procedure as well as on the final freezing temperature, intra- and extracellular ice formation can occur. Intracellular ice crystals may induce mechanical stress on cell walls provoking partial cell damage, which may lead to a certain homogenization of the tissue and, hence, reduction of scattering. After thawing, cell wall ruptures can provoke blood drain and oxidation of deoxyhemoglobin, reducing light absorption in the

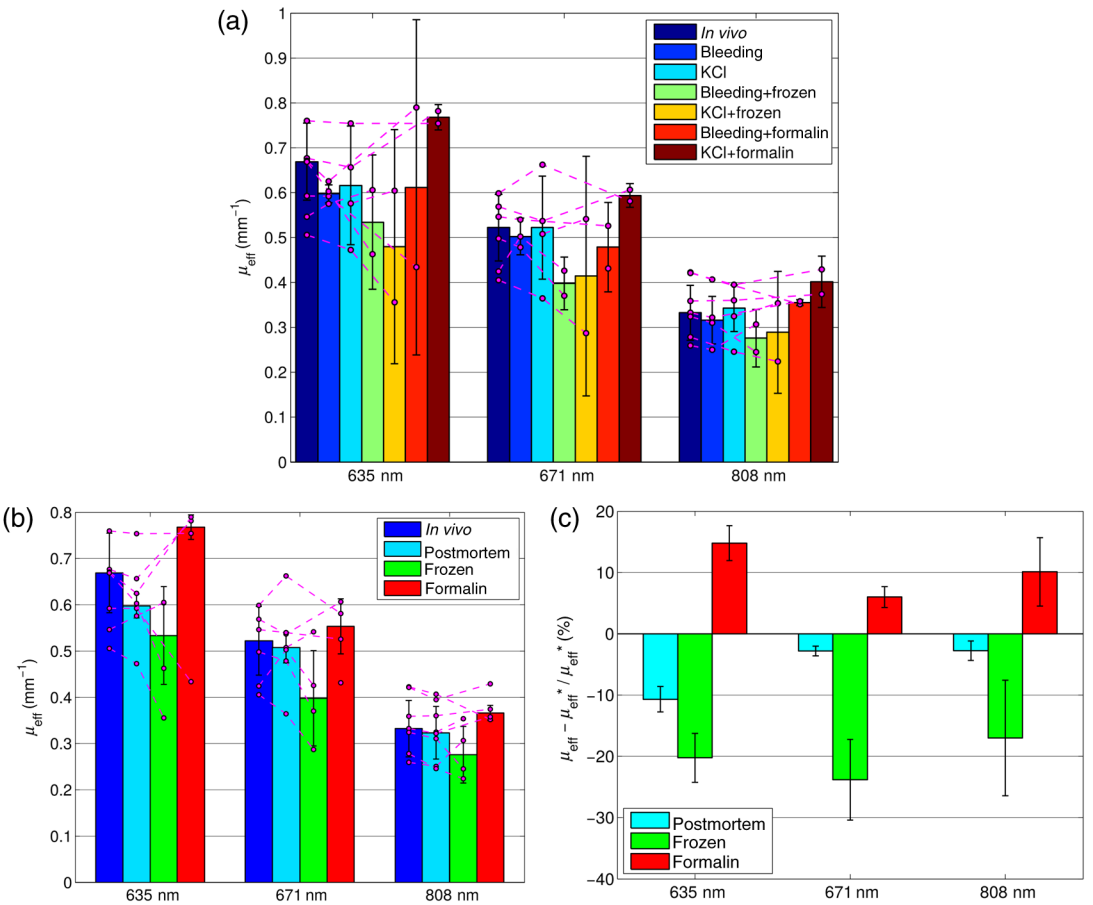

Fig. 3 The effective attenuation coefficient μ_{eff} as function of the wavelength is shown in (a) for all experimental conditions and in (b) for all tissue conditions, i.e., a reduced set of data from (a). Magenta markers represent μ_{eff} obtained from each animal; dashed lines connecting the evolution of μ_{eff} for each animal during the euthanasia and tissue storing procedure. The relative change in μ_{eff}, $(\mu_{eff} - \mu_{eff}^*)/\mu_{eff}^*$, where μ_{eff}^* is the *in vivo* value, is shown in (c) and was computed for all conditions from the averaged μ_{eff}.

range of 600 to 800 nm.[28] In our experiments, this effect may have been further amplified by the fact that the brain was left in the cranial cavity the entire study. The volumic expansion of the brain tissue during slow freezing was constrained by the skull, thus increasing mechanical stress on the cells. Extracellular ice formation may have changed solute concentrations, which can lead to cellular dehydration provoking protein denaturation,[29] which may also have affected tissue optical properties.[4]

It remains unclear what the partially controversial results reported in the literature (Table 3) can be attributed to. However, overall scattering and absorption are likely to decrease when slowly freezing bulky tissue to -20°C, which is also reflected in our observations and those made with different tissues.

4.2 *Tissue Fixation in Formalin*

Formalin fixation is a preparation method widely used for handling tissue specimens, especially for long-term storage. However, very little is known about its effect on tissue optical

Table 2 Effective attenuation, μ_{eff}, absorption, μ_a, and reduced scattering, μ_s', coefficients measured at 635, 671, and 808 nm for different conditions (*in vivo*, postmortem, frozen, and formalin). Uncertainties are given in parentheses.

		μ_{eff} (cm^{-1})			μ_a (cm^{-1})			μ_s' (cm^{-1})		
Condition	Animals	635 nm	671 nm	808 nm	635 nm	671 nm	808 nm	635 nm	671 nm	808 nm
In vivo	7	6.7 (0.9)	5.2 (0.7)	3.3 (0.6)	1.1 (0.2)	0.8 (0.2)	0.5 (0.1)	12.8 (1.0)	10.7 (0.9)	6.2 (0.5)
Postmortem	8	6.0 (0.3)	5.1 (0.3)	3.2 (0.6)	0.9 (0.1)	0.8 (0.1)	0.5 (0.1)	12.0 (0.3)	10.5 (0.4)	6.1 (0.5)
Frozen	4	5.3 (1.1)	4.0 (1.0)	2.8 (0.6)	0.8 (0.2)	0.5 (0.2)	0.4 (0.1)	11.2 (1.3)	9.2 (1.3)	5.7 (0.6)
Formalin	4	7.7 (0.3)	5.5 (0.6)	3.7 (0.2)	1.3 (0.1)	0.9 (0.1)	0.6 (0.1)	14.0 (0.3)	11.0 (0.7)	6.5 (0.1)

properties. In previous studies, an increase in optical scattering was observed after fixation, which is related to the cross-linking of proteins during tissue fixation creating a more scattering media, while absorption mainly remains unaltered.[9,10,30] To our knowledge, there is no study where optical properties were directly measured before and after tissue fixation, but only under conditions of tissue coagulation[4,7] or direct dehydration.[11] These results are presented in Table 3.

Formaldehyde acts as a cross-linking agent at the molecular level by linking together soluble and structural proteins,[31,32] resulting in (1) tissue shrinkage by dehydration and (2) alterations in tissue structural properties. Tissue shrinkage decreases the diameter of cells and aggregates responsible for scattering. Following Mie's scattering theory, μ_s is proportional to the square of the scattering centers' diameters, which should lead to a decrease in the scattering coefficient and anisotropy factor in the case of tissue shrinkage. For small diameter changes, however, μ_s' remains approximately constant, since μ_s and g decrease at the same time.

It remains unclear how changes in tissue structural properties induced by formalin fixation concretely affect light scattering. Furthermore, the dehydration of cells during the fixation process is also likely to change the refractive index. While it is ~1.38 for fresh tissue,[33,34] the refractive index of dehydrated cells increases to 1.50 to 1.55.[35] Even a small difference in the refractive index may yield a larger reduced scattering coefficient, since $\mu_s' \propto (n-1)^2$ or larger.[27] Accordingly, values of reduced scattering coefficients are likely to increase by 70% when n increases from 1.38 to 1.50.

Tissue dehydration and shrinkage resulting from the fixation process also lead to an increased concentration of chromophores. Thus, the observed increase in the absorption coefficient may be a result of denser packing of cells due to shrinkage of the tissue samples while the number of chromophores remains constant.[4] Hsiung et al.[30] investigated changes of the optical properties of hamster cheek pouch at 800 nm when preserving it in a 10% neutral-buffered formalin solution. Besides tissue shrinkage, they found both increasing and decreasing scattering signals depending on the tissue type and an increase in the overall contrast between tissue architectural features during the fixation process over 18 h. Aung et al.[10] investigated the refractive index and scattering properties in tissues of prostate cancer. The comparison of reduced scattering coefficients obtained from fixated and frozen samples leads to opposite results: in nuclear regions, μ_s' was found to be higher in fixated than in frozen tissue, whereas the opposite was concluded for the samples from non-nuclear regions. These different results may be due to large uncertainties in their determination of g. Gnanadesigan et al.[36] investigated the effect of temperature and fixation on the optical properties of atherosclerotic tissue with the help of optical coherence tomography. Their results suggest that tissue fixation and temperature do not introduce changes in the attenuation coefficient of coronary arteries, yet they observed increased image intensity after fixation indicating a larger reduced scattering coefficient. As a consequence of an approximately constant μ_{eff}, their results would mean that μ_a decreased during the fixation process. Gabrecht et al.[37] showed blue-violet excited autofluorescence of normal and cancerous human bronchial tissue to be increased after formaldehyde fixation, which is an indication for a lowered absorption. However, the only difference in the spectra was localized in the absorption range of hemoglobin around 530 to 560 nm. It was shown elsewhere[38] that hemoglobin's absorption decreases significantly and blood vessels become invisible in OCT[30] following the formaldehyde fixation process.

In summary, the knowledge of the effects of formaldehyde fixation on tissue optical properties is very scarce. There are indications that the overall scattering increases due to protein

Table 3 A summary of literature values about the relative changes in effective attenuation, μ_{eff}, absorption, μ_a, and reduced scattering, μ_s', after tissue treatment, i.e., freezing or formalin-fixation. Relative changes are given as averaged values of the respective optical parameter within the wavelength range or at the distinct wavelengths, λ.

Literature	Tissue	Treatment	λ (nm)	$\delta\mu_a$ (%)	$\delta\mu_s'$ (%)	$\delta\mu_{\text{eff}}$ (%)
Salomatina[13]	Mouse ear (*in vivo*)	Frozen-thawed (–25°C)	600 to 850	–25	–20	–25
Roggan[3]	Porcine liver (*in vitro*)	Slow-frozen (–20°C)	600 to 710	–10	–20	–15
		Shock-frozen (77 K)		~0	–5	–3
Chan[8]	Rat jejunum (*in vitro*)	Shock-frozen (77 K)	600 to 800	–55	–10	–30
Zhu[11]	Porcine liver (*in vitro*)	Frozen and dehydrated (–20/20°C)	633	+30	+390	+100
		Frozen and dehydrated (–20/37°C)		+150	+10	+110
Yaroslavsky[7]	Human brain, white matter (*in vitro*)	Coagulated (saline bath, 80°C)	600 to 800	+250	–30	+35
	Human brain, gray matter (*in vitro*)			+400	+90	+280
Çilesiz[4]	Human aorta (*in vitro*)	Coagulated (water bath, 100°C)	630, 1065	+40	+7	+25
Wood[9]	Porcine myocardium (*in vitro*)	Formalin-fixated	635	~0	(+40)[a]	(+20)
This study	Rabbit brain (*in vivo*)	Slow-frozen (–20°C)	635 to 810	–30	–10	–20
		Formalin-fixated		+15	+5	+10

[a]Only $\delta\mu_s$ was investigated in this study. $\delta\mu_s'$ was computed from $\delta\mu_s$ by assuming $g = 0.9 = \text{const}$.

linking, tissue dehydration, and shrinkage. Tissue shrinkage itself may also increase the density of chromophores leading to higher absorption if chromophores remain intact during and after formaldehyde treatment. Light absorption of hemoglobin derived from porphyrin rings is lowered by formaldehyde, but mainly at wavelengths <600 nm. On the contrary, coagulation of human brain tissue increases the absorption coefficient to a larger extent than the reduced scattering, which was also observed in our study.

4.3 *Effects of Structural Changes in the Brain on the Optical Coefficient After Long-Term Storage*

The repositioning of the catheters in the rabbit brain for the measurement after long-term storage may introduce an additional uncertainty in the absolute values of the optical coefficients obtained from data fitting and, hence, their relative changes after tissue storage. Although care was taken to reintroduce the catheters in the same positions as were originally used in the measurements prior to long-term storage, there were small differences (a few millimeters) in the catheter trajectories between prior and poststorage measurements. The recomputation of the catheter coordinates from sets of x-ray images obtained poststorage was supposed to yield, within the accuracy of the method itself, correct relative distances between the light source and detector. Nevertheless, an altered trajectory also implies a possible change of the surrounding tissue and, therefore, a change in local optical coefficients and fluence rate.

It remains unclear to what extent this effect may bias the results, since no histological processing of the tissue was performed. However, multiple measurements along the catheter trajectories should reduce the impact of the local tissue inhomogeneities and optical properties on the results. Furthermore, the effects of the structural changes in the surrounding tissue may also be one possible explanation of the changes in μ_{eff} from a single animal between prior and poststorage measurements [see magenta dots in Figs. 3(a) and 3(b)].

5 Conclusions

Light-based treatments of diseases depend, among other things, on how and to what extent the light is distributed in biological material. Thus, knowledge of the optical properties of tissues is crucial, as is knowledge of how tissue preparation and storing processes impact them. The objective of the present study was to quantify how light attenuation in brain tissue changes between *in vivo* and postmortem rabbit heads, and how it could be affected by histological tissue processing or by the animal sacrifice and subsequent tissue storage.

We demonstrated that μ_{eff} is not very sensitive to the method of animal sacrifice (exsanguination or injection of KCl). We also showed that μ_{eff} decreases as wavelengths increase. When passing from *in vivo* to postmortem conditions, the decrease in μ_{eff} was largest at 635 nm (up to 10%), whereas at longer wavelengths, it was only 5%. Tissue freezing was confirmed to significantly alter tissue optical properties: μ_{eff} decreased on average by 15 to 25% at all wavelengths after storage of the rabbit heads at -20°C for six weeks, with $\delta\mu_{\mathrm{eff}}$ becoming smaller with increasing wavelength. On formalin-fixated samples, our measurements showed an increase in μ_{eff} by 5 to 15% after having stored the rabbit heads in formaldehyde for six weeks, but it remained unclear how changes in tissue structural properties induced by formalin fixation concretely affected light scattering.

We demonstrated a convincing fit between optical coefficients μ_{a} and μ_{s}', absorption and reduced scattering on one hand, and experimental results on the other hand. We could, however, not precisely identify which optical coefficient was the crucial factor determining changes in μ_{eff} in our various experiments, although we observed that overall scattering and absorption decreased when slowly freezing brain tissue to -20°C and that they might increase when fixating it in formalin. Finally, we interpreted the influence of the experimental constraints on the measured data by Monte Carlo simulations.

Acknowledgments

The authors thank O. Beslac, D. Mettler, and D. Zalokar, Experimental Laboratory ESI, University of Bern, Switzerland, for assistance during animal preparation and data collection. We also thank Professor S. Jakob and Professor H. van den Bergh for their helpful support in realizing this study. This work was supported in part by the CTI projects 13758.1 and 14660.1, the Swiss National Science Foundation, project 205320_147141/1, and the J. Jacobi grant.

References

1. T. Vo-Dinh, *Biomedical Photonics Handbook*, CRC Press, Mortimer Street, London (2003).
2. S. L. Jacques, C. A. Alter, and S. A. Prahl, "Angular dependence of HeNe laser light scattering by human dermis," *Laser Life Sci.* **1**(4), 309–333 (1987).
3. A. Roggan et al., "Effect of preparation technique on the optical parameters of biological tissue," *Appl. Phys. B: Laser Opt.* **69**(5), 445–453 (1999).
4. I. F. Çilesiz and A. J. Welch, "Light dosimetry: effects of dehydration and thermal damage on the optical properties of the human aorta," *Appl. Opt.* **32**, 477–487 (1993).
5. J. Pickering et al., "Double-integrating-sphere system for measuring the optical properties of tissue," *Appl. Opt.* **32**(4), 399–410 (1993).
6. A. Nilsson et al., "Changes in optical properties of human whole blood in vitro due to slow heating," *Photochem. Photobiol.* **65** (2), 366–373 (1997).
7. A. N. Yaroslavsky et al., "Optical properties of selected native and coagulated human brain tissues in vitro in the visible and near infrared spectral range," *Phys. Med. Biol.* **47**(12), 2059–2073 (2002).
8. E. Chan, T. Menovsky, and A. Welch, "Effects of cryogenic grinding on soft-tissue optical properties," *Appl. Opt.* **35**(22), 4526–4532 (1996).
9. M. Wood et al., "Effects of formalin fixation on tissue optical polarization properties," *Phys. Med. Biol.* **56**(8), N115–N122 (2011).
10. H. Aung et al., "On alterations in the refractive index and scattering properties of biological tissue caused by histological processing," *Proc. SPIE* **8592**, 85920X (2013).
11. D. Zhu, Q. Luo, and J. Cen, "Effects of dehydration on the optical properties of in vitro porcine liver," *Laser Surg. Med.* **33**(4), 226–231 (2003).
12. R. Graaff et al., "Optical properties of human dermis in vitro and in vivo," *Appl. Opt.* **32**(4), 435–447 (1993).
13. E. Salomatina and A. Yaroslavsky, "Evaluation of the in vivo and ex vivo optical properties in a mouse ear model," *Phys. Med. Biol.* **53**(11), 2797–2807 (2008).
14. E. Angell-Petersen, H. Hirschberg, and S. J. Madsen, "Determination of fluence rate and temperature distributions in the rat brain; implications for photodynamic therapy," *J. Biomed. Opt.* **12**(1), 014003 (2007).
15. L. O. Svaasand and R. Ellingsen, "Optical properties of human brain," *Photochem. Photobiol.* **38**(3), 293–299 (1983).
16. B. Hallacoglu et al., "Absolute measurement of cerebral optical coefficients, hemoglobin concentration and oxygen saturation in old and young adults with near-infrared spectroscopy," *J. Biomed. Opt.* **17**(8), 081406 (2012).
17. L. Wang and H. Wu, *Biomedical Optics: Principles and Imaging*, John Wiley & Sons, Inc., Hoboken, New Jersey (2007).

18. C. Zhu and Q. Liu, "Review of Monte Carlo modeling of light transport in tissues," *J. Biomed. Opt.* **18**(5), 050902 (2013).
19. L. Wang, S. L. Jacques, and L. Zheng, "MCML—Monte Carlo modeling of light transport in multi-layered tissues," *Comput. Methods Programs Biomed.* **47**(2), 131–146 (1995).
20. A. Ishimaru, *Wave Propagation and Scattering in Random Media*, Academic Press, New York (1978).
21. L. G. Henyey and J. L. Greenstein, "Diffuse radiation in the galaxy," *Astrophys. J.* **93**, 70–83 (1941).
22. B. J. Tromberg et al., "A mathematical model for light dosimetry in photodynamic destruction of human endometrium," *Phys. Med. Biol.* **41**(2), 223 (1996).
23. Q. Fang, "Mesh-based Monte Carlo method using fast raytracing in Plücker coordinates," *Biomed. Opt. Express* **1**(1), 165–175 (2010).
24. Q. Fang and D. A. Boas, "Tetrahedral mesh generation from volumetric binary and gray-scale images," in *Proc. IEEE Int. Symp. on Biomedical Imaging: From Nano to Macro*, pp. 1142–1145, IEEE Press, Piscataway, NJ (2009).
25. W. Krause, *Die Anatomie des Kaninchens in topgraphischer und operativer Rücksicht*, Verlag von Wilhelm Engelmann, Leipzig (1884).
26. A. Custo et al., "Effective scattering coefficient of the cerebral spinal fluid in adult head models for diffuse optical imaging," *Appl. Opt.* **45**(19), 4747–4755 (2006).
27. R. Graaff et al., "Reduced light-scattering properties for mixtures of spherical particles: a simple approximation derived from Mie calculations," *Appl. Opt.* **31**, 1370–1376 (1992).
28. V. Tuchin, *Tissue Optics: Light Scattering Methods and Instruments for Medical Diagnosis*, SPIE Press, Bellingham, Washington (2007).
29. F. Franks, R. Hatley, and H. Friedman, "The thermodynamics of protein stability: cold destabilization as a general phenomenon," *Biophys. Chem.* **31**(3), 307–315 (1988).
30. P.-L. Hsiung, P. Nambiar, and J. Fujimoto, "Effect of tissue preservation on imaging using ultrahigh resolution optical coherence tomography," *J. Biomed. Opt.* **10**(6), 064033 (2005).
31. A. G. E. Pearse, *Histochemistry: Theoretical and Applied*, 4th ed., Church Livingstone Press, New York (1991).
32. M. Abe et al., "The changes in crosslink contents in tissues after formalin fixation," *Anal. Biochem.* **318**(1), 118–123 (2003).
33. H. Li and S. Xie, "Measurement method of the refractive index of biotissue by total internal reflection," *Appl. Opt.* **35**, 1793–1795 (1996).
34. J. Dirckx, L. Kuypers, and W. Decraemer, "Refractive index of tissue measured with confocal microscopy," *J. Biomed. Opt.* **10**(4), 044014 (2005).
35. D. Cook, *Cellular Pathology: An Introduction to Techniques and Applications*, 2nd ed., Scion Publishing Ltd., Banbury, Oxfordshire (2006).
36. M. Gnanadesigan et al., "Effect of temperature and fixation on the optical properties of atherosclerotic tissue: a validation study of an ex-vivo whole heart cadaveric model," *Biomed. Opt. Express* **5**, 1038–1049 (2014).
37. T. Gabrecht, S. Andrejevic-Blant, and G. Wagnières, "Blue-violet excited autofluorescence spectroscopy and imaging of normal and cancerous human bronchial tissue after formalin fixation," *Photochem. Photobiol.* **83**(2), 450–459 (2007).
38. R. Farbiszewski, E. Skrzydlewska, and A. Roszkowska, "Formaldehyde-induced modification of hemoglobin in vitro," *Acta Biol. Hung.* **49**(2–4), 345–352 (1998).

Biographies of the authors not available.